inter.noise
HAMBURG 2016

Tyre Contact Forces on a Particulate Road Surface

Roger James PINNINGTON
U.K.

ABSTRACT

Determination of the contact forces in road tyre interaction is the central problem in all aspects of road tyre interaction: i.e. noise, energy loss and friction. The time varying contact forces and the non-linear force-displacement are found in a new straight-forward procedure that utilises a particle-envelope model. A routine divides a surface profile into equal search intervals in which the highest peaks are identified, from which the mean particle and the envelope properties for the search interval are obtained. The process is repeated at geometrically decreasing search intervals until the level of the data resolution. The properties defining the surface for contact calculation are: the mean envelope, the mean contact length and the mean interval. The contact stiffness of a uniform peak array due to indentation in the rubber, and tyre deflection is calculated. The surface geometric properties are then combined with the contact stiffness to give the mean deflections in terms of the tyre parameters and vertical load. The time varying contact forces are then given directly from the peak profiles using a new but simple contact relationship.

Keywords: contact forces, contact stiffness, surface modelling

1. INTRODUCTION

Determination of the contact forces in road-tyre interaction is the central problem in all aspects of road tyre interaction. However due to complexity of the surface and the non-linearity of the contact this is usually only attempted with numerical procedures relying on detailed input data e.g. (1). However the approach here, from (2), relies more on mathematical modelling in terms of averaged surface parameters with a view to gain an understanding of the physics of the interaction and make predictions of time averaged response.

Road-tyre contact is associated with the different surface wavelengths as illustrated in Fig. 1. When, as in Fig. 1a, the surface wavelength λ is greater than the contact patch of length L_s, the contact forces act in phase as a single point on the tyre, transmitting low frequency vibration and noise to the vehicle interior. If the surface is magnified as in Fig.1b, the contact, acting over a number of discrete points at the peaks of the road stones, is responsible for high frequency road-tyre noise. Further magnification of the road profile, as in Fig.1c, shows the stone texture, where wavelengths less than 1mm are responsible for friction.

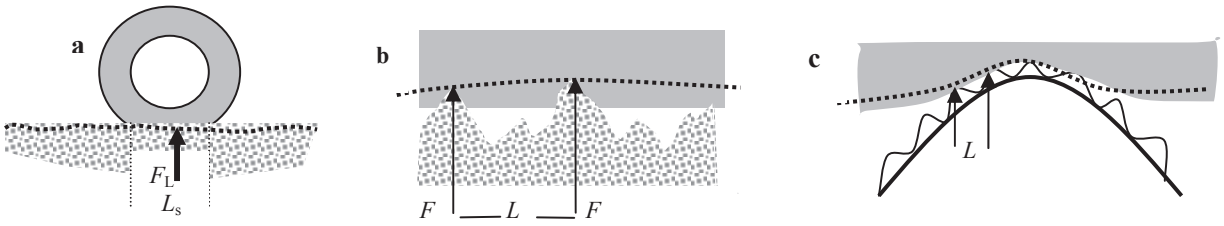

Figure 1- Contact between a tyre and a road surface: …….. peak envelope,
a. long wavelengths , **b**. stone profile. **c**. stone texture

A procedure to find the contact forces under a rolling tyre is presented in four stages. First, the contact stiffness of a uniform peak array from: indentations in the rubber tread, and also tyre carcass deflection, is described by some new simplified expressions. Second, a routine divides a single surface profile into equal search intervals, in which the highest peaks are identified. These are used to obtain the parameters for the interval, i.e. the mean envelope and the mean interval. The process is repeated at geometrically decreasing search intervals until the level of the data resolution, thereby describing the profile by a set of envelopes. The surface is ultimately described by the 'strip profile', obtained by selecting the highest points across the profiles of one stone's width. The third stage is to combine the strip profile envelopes with the contact stiffness expressions, yielding the non-linear stiffness-displacement, and force-displacement relationships for the chosen road-tyre combination. The final stage is to use these relationships to find the contact forces under a rolling tyre and to make a linear wave equation for the interaction.

2. STATIC CONTACT FOR A UNIFORM ARRAY OF PEAKS

The deformation of an elastic tyre on a rough surface is considered to be of two sorts: local *indentation* of contacts on an elastic half-space, and the *deflection* of the unsupported tyre belt between contact points. An approximate relationship between contact force and *indentation* on a single particle of arbitrary shape is presented. The result is then extended for indentation on a uniform array of equal independent projections. The effect of surface 'saturation', when the rubber fills the intermediate space between peaks, is then included. Finally the uniform array stiffness due to the two sorts of *deflection*, bending and tension-shear is included.

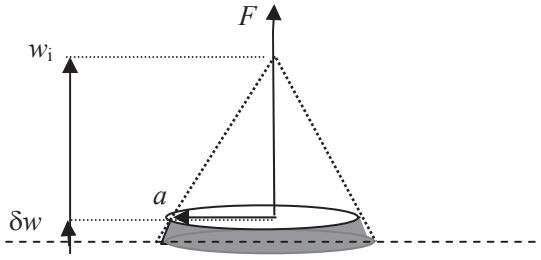

Figure 2- Indentation into a half-space for a general profile

A force F acts on a flat disc of radius a, seen in Fig.2 on an elastic material of Young's modulus E and Poisson's ratio ν, where $E^*=E/(1-\nu^2)$. The contact stiffness K_I is proportional to the contact radius a as equation 1a, (3) :

$$\frac{\mathrm{d}F}{\mathrm{d}w} = K_I = 2E^* a, \quad F = E^* \int_0^{w_i} 2a\mathrm{d}w \tag{1a,b}$$

If the disc is depressed δw the displaced volume $2\pi a^2\,\delta w$ would be the same as for indentation δw of the subtended cone also displayed, suggesting that the contact stiffness of any profile can be defined simply from the diameter $2a$ across the plane of contact as Eq.(1a). The contact force F is then given from the integral of contact stiffness with respect to penetration depth w_i as Eq.(1b), i.e. proportional to the area of indentation. This approximation was applied to exact formulations(2,3) for a sphere and cone, giving a fair fit, confirming its use for projections of any shape.

The single point result can be extended for a uniform two dimensional array of identical peaks of spacing L, loaded with a uniform pressure p, as seen in Fig.3. Assuming that the points are well separated i.e. $d<<L$ the force/point becomes $F=pL^2$, giving a contact stiffness $K_i = \mathrm{d}p/\mathrm{d}w = K_I/L^2$. A general expression to include the effect of surface saturation when d approaches L is given in (2) i.e.

$$\frac{\mathrm{d}p}{\mathrm{d}w} = K_i = \frac{K_I}{L^2\left(1-\left(d\ /L\ \right)^2\right)^2} \tag{2}$$

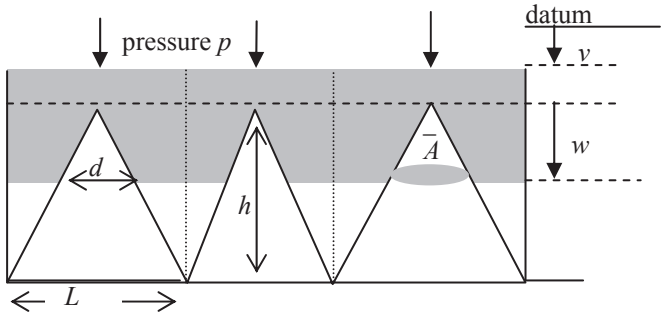

Figure 3- Diagonal section through an array of identical particles

The flexibility of the tyre belt also allows it settle arround the surface asperities, contributing to the total displacement. The *deflection* is assumed to have have two parts shown in Fig. 4: bending w_b and a tension-shear combination w_{ts} controlled by the tension N_x and bending stiffness B_x, (2). These yield the array stiffness K_{ts} and K_b for tension-shear and bending. The maximum deflection w_d at the mid-point x,y=0 is given as the sum of the two components i.e. $w_{ts}+w_b$ arising from a pressure p:

$$w_d = \frac{p}{K_d} = \frac{p}{K_{ts}} + \frac{p}{K_b}, \quad K_{ts} = \frac{2\pi^2 \left(N_x + S_x\right)}{L^2}, \quad K_b = \frac{32\pi^4 B_x}{L^4} \tag{3a,b,c}$$

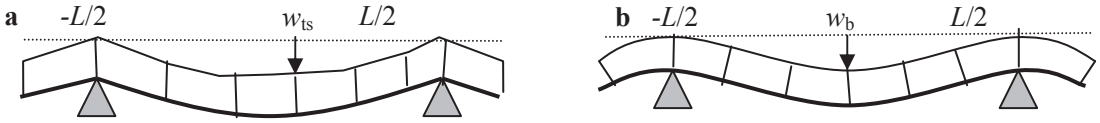

Figure 4- Belt deflection**, a.** tension-shear controlled**, b.** bending controlled

3. PEAK ENVELOPE DECOMPOSITION

In principle, if the surface profile were known, the contact forces for a tyre could be found by application of Eq.(2,3) into the integral of Eq.(1). But it is first necessary to define the surface in terms of the penetration depth using the envelopes passing through the peak tips, representing the tyre rubber surface settling into the road surface with increasing load. The envelopes are decomposed into a set of single sided components that sum together to completely describe a road profile at any position x. The peak envelope identification procedure is demonstrated and applied to a set of three-dimensional data, measured from the road surface of the B56, near Düren, Germany.

Each peak peak envelope w_n takes a similar form to the fractal Weierstrass-Mandlebrot (W-M) function $w_n(x)$ introduced in (4), i.e.

$$w_n(x) = \sum_{n=0}^{n} \tilde{w}_n, \quad \tilde{w}_n = W_n \left(\sin\left(k_n x + \phi_n\right) + 1\right), \; W_n = \frac{W_0}{\gamma^{nH}}, \; k_n = \frac{2\pi}{\lambda_n}, \; k_n = \gamma^n k_0 \tag{4}$$

Each envelope w_n is the summation of $0 \le n$ sinewave components $\tilde{w}_n$ of geometrically decreasing wavelength λ_n. The full profile w_N is thus the sum over components $0 \le n \le N$. The components $\tilde{w}_n$ are sinewaves offset by unity, so that the envelope w_n is built in positive steps of mean value W_n.

Fig.5 is used to illustrate the envelope identification procedure for a measured surface profile w_N, where increasing envelope number n describes how the tyre progressively settles over the surface from initial contact at n=0 until complete saturation at n=N. Each envelope w_n is decomposed into components $\tilde{w}_n$, $0 \le n$, as for the W-M summation of Eq.(4), though they are no longer offset sinewaves, but offset triangular quasi-periodic sequences of mean spacing L_n. However, the notation of Eq.(4) is retained to assist the interpretation. The frequency multiplier γ for the peak search interval L_{sn}, is set as γ=2 to give integer steps. The search interval L_{sn} is the number of samples q_n, scaled by the data resolution δx, i.e.

$$L_{sn} = \delta x . q_n, \quad q_n = \gamma^{N-n}, \; \gamma = 2, \quad n = 0,1,2,3..N \tag{5a,b}$$

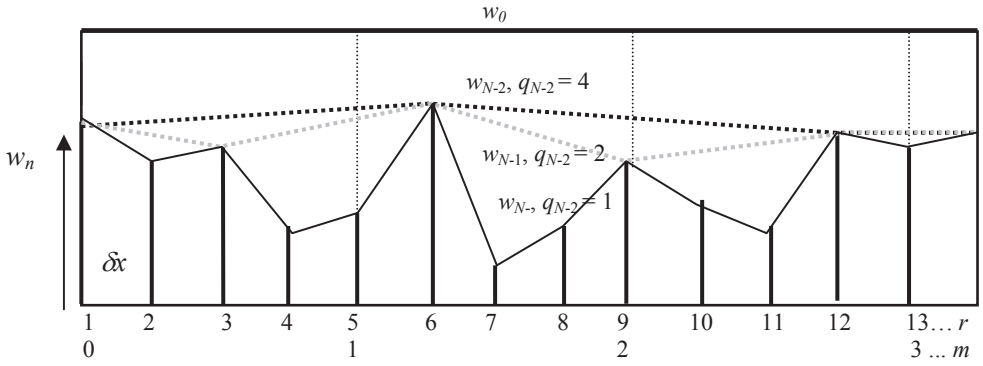

Figure 5- Envelopes w_n and search intervals q_n

The profile w_N in Fig.5 of r=13 samples, is divided into a sequence of m=0,1,2…M_n search intervals, each of q_n samples. The samples are counted by $r=mq_n+q$, where q=1,2,3..q_n, counts the incomplete interval. For example, Fig.5 shows the search scheme for q_{N-2} =4, i.e. with the profile divided into intervals of four points by the vertical lines. In the first interval (m=0), the largest peak is identified as the first point. Likewise in the second interval (m=1), the largest peak is seen to be the second point, and so on, linked by the envelope labelled w_{N-2}. The subsequent search intervals for n>0 are found by progressively halving the previous intervals. The envelope of the next smaller set of peaks labelled w_{N-1}, for q_{N-1} =2, is also shown, while q_N =1 will return the full profile w_N.

To ensure that the envelopes are correctly ordered, peaks in level n are only registered if in the middle third of the interval L_{n-1}. Thus the largest envelope is w_0 at the highest peak tips, while the smallest envelope w_N reaches down between the peaks to the bottom of the troughs. The most important intermediate envelope w_p is at the 'particle level' $n=p$, when the search interval is small enough to span most of the particle peaks without dropping between. For $n>p$ there are no more significant peaks, and the search routine finds only local maxima in the middle third of the interval until completely filling out the profile at $n=N$.

The increment between subsequent envelopes is called the component $\tilde{w}_n$, seen in Fig.5, as a sequence of downward triangles i.e.

$$\tilde{w}_n(x) = w_n(x) - w_{n-1}(x), \quad w_n = \sum_{n=0}^{n} \tilde{w}_n \tag{6a,b}$$

The mean component W_n (referred to as the 'step'), and mean envelope $\overline{w}_n$, are averages of Eq.(6a,b) taken over the profile length, i.e.

$$W_n = \overline{w}_n - \overline{w}_{n-1} \tag{7}$$

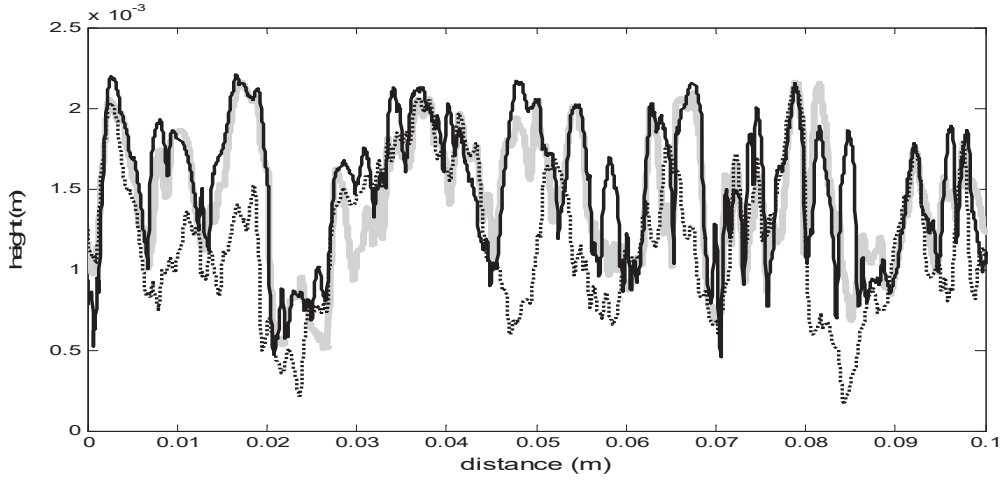

Figure 6- Road profiles: ····· single profile, ——— triple profile, ——— full profile

An envelope decomposition was made on 1.4m of a single measured profile of which only 0.1m is shown (a typical length of a tyre contact patch), labelled 'single' in Fig.6. However the 'single profile'cannot be used for contact calculations as it does not usually pass through the highest points of each peak, therefore a correction was made (2), by constructing what is termed the 'strip profile' w_N which has the true peak heights, and also trough depths that are correct on average, where the strip width Δ, corresponds to the width of the largest particle, in this case Δ=0.01m.

Three strip profiles, from different numbers of profiles across the strip width, are compared in Fig. 6. The 'single' profile is the uncorrected profile at the strip centre line. The 'triple' profile is calculated from only three profiles, at the strip centre line and either side at 3.3mm. The 'full' profile is calculated from fifty profiles spaced 0.2mm across the strip width of 10mm. The resulting 'triple' profile and 'full' profile' are very similar, both in the peak and the trough levels.

The resulting mean properties: envelope $\overline{w}_n$, step W_n, and contact diameter d_n are given in Fig.7. The mean properties of the three profiles are very similar, with the envelopes falling slowly form 2.5mm at n=0 to 1mm at n=9, i.e. at surface saturation. There are some differences in the region of the particle levels n=4, 5, where the steps of the 'single profile' are about 0.5mm greater than those of the 'triple profile' and 'full profile'. This difference caused by the error in the particle shape, is seen mainly at search intervals close to the particle spacing. The steps increase for levels n>4 as the envelopes begin the penetrate between the particles. Above n=7, there are no more particles; the search interval is halved each time and so the depth is halved on average from the triangular geometry, giving the linear relationship.

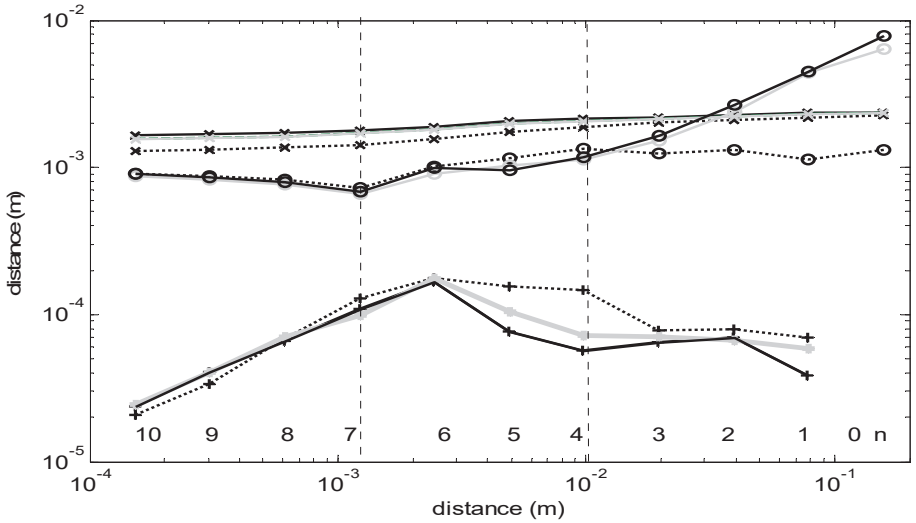

Figure 7- Mean profile properties v level n: ▪▪▪▪▪▪▪ single profile, ——— triple profile, ——— full profile: x----x envelope, +-----+ step; o-----o contact diameter .

In summary, from the mean properties for the steps and contact diameter it appears that the 'triple' profile formed from three profiles across the strip, will adequately describe the surface.

4. CONTACT STIFFNESS v DISPLACEMENT

The contact stiffness' for a uniform array can now be combined with the envelope functions to calculate the contact stiffness of a flat tyre on a rough surface as a function of the envelope level n, as defined by the displacement step W_n at pressure P_n, where W_n is the sum of the displacement steps from tension-shear, W_{tsn}, bending W_{bn} and indentation W_{in}. i.e.

$$W_n = W_{tsn} + W_{bn} + W_{in} \tag{8}$$

The pressure acts equally on each deformation type, thus division of Eq.(8) by P_n, yields the combined stiffness K_n in terms of contributions from tension-shear K_{tsn}, bending K_{bn} and indentation K_{in} i.e.

$$K_n = \left(\frac{1}{K_{in}} + \frac{1}{K_{tsn}} + \frac{1}{K_{bn}} \right)^{-1}, \quad K_n = \frac{P_n}{W_n}, \; K_{in} = \frac{P_n}{W_{in}}, \; K_{tsn} = \frac{P_n}{W_{tsn}}, \; K_{bn} = \frac{P_n}{W_{bn}} \tag{9}$$

The uniform array stiffness' for indentation, tension-shear, and bending in Eqs.(2,3) are rewritten in Eq.(10), using the mean contact diameter d_n, and mean interval L_n of the non-uniform arrays, i.e.

$$K_{in} = \frac{E^* d_n}{L_n^2\left(1-\left(d_n/L_n\right)^2\right)^2},\ K_{tsn} = \frac{2\pi^2\left(N_x + S_x\right)}{L_n^2},\ K_{bn} = \frac{32\pi^4 B_x}{L_n^4} \tag{10a,b,c}$$

The mean contact diameter d_n, and mean interval L_n for the three profiles in Fig.7 are applied to Eq.(10) as a simple means of representing surfaces of different roughness. The material properties are typical for a car tyre are all taken from (5): the tread rubber Young's Modulus E=3x10^{7}N/m^2, the tension/length N_x=3x10^{4}N/m, the shear force/length S_x=1.5x10^{5}N/m, and the bending stiffness/length B_x=90Nm; thus yielding the contact stiffness in Fig.8, given as a function of the mean displacement as the sum of the steps W_n:

$$\overline{w}_n = \sum_{n=1}^{n} W_n \tag{11}$$

Noting that the pressure P_n is common to each deformation type, the corresponding $\overline{w}_{in}, \overline{w}_{tsn}, \overline{w}_{bn}$, are found from the stiffness terms of Eq.(9) i.e.

$$\overline{w}_{in} = \sum_{n=1}^{n} \frac{K_n}{K_{in}} W_n,\ \ \overline{w}_{bn} = \sum_{n=1}^{n} \frac{K_n}{K_{bn}} W_n,\ \ \overline{w}_{tsn} = \sum_{n=1}^{n} \frac{K_n}{K_{tsn}} W_n \tag{12a,b,c}$$

Most tyres have a tread pattern giving an added compliance to the contact. If the tread slots are of depth h, the corresponding stiffness/area of the slotted tread K_{tr} is E/h. Assuming a typical block height of h=0.01m, K_{tr} =3x10^{9}N/m^2/m, displayed in Fig.8 as the constant dashed line.

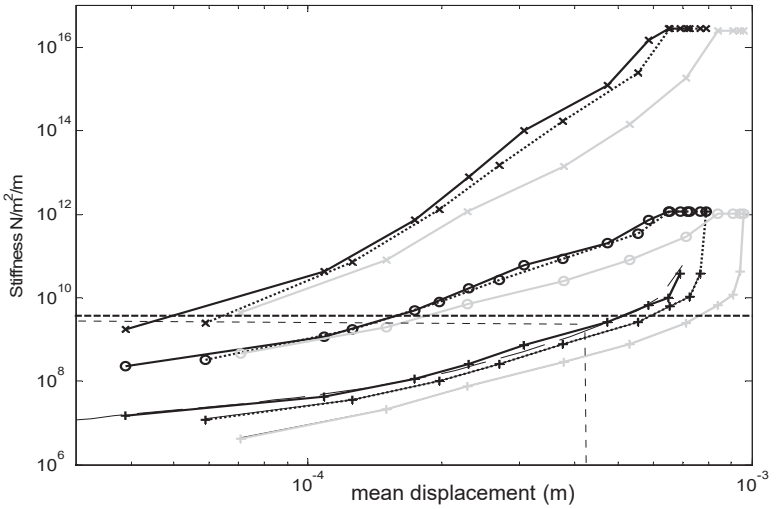

Figure 8- Contact stiffness v mean displacement $\overline{w}_n$, ——— single profile, ... triple profile, ——— full profile, x---x bending, o---o tension-shear, +---+ indentation, – – – tread block, _ _ _ fit to full profile

Each curve has ten markers from left to right identifying the stiffness as it increases rapidly with displacement from initial contact at n=1 to n=10, at surface saturation. The stiffness curves are in three groups for bending K_{bn}, tension-shear K_{tsn} and indentation K_{in}. The bending stiffness is the greatest and the indentation stiffness is lowest and so most responsible for the combined displacement. The surface saturates and stiffness rapidly at a mean envelope displacement of 1mm for the single profile but only 0.7mm for the smoother 'full profile'. The stiffness likewise increases with surface smoothness, thus the full profile is stiffest, and the single profile is the softest.

An empirical relationship between K_d and envelope displacement is obtained from K_n in Fig.8 using the asymptotic slopes n_1, n_2 at small and large displacements, i.e.

$$K_d = \frac{C_1\overline{w}^{n_1} + C_2\overline{w}^{n_2}}{1-\overline{w}^{n_3}},\quad \overline{w} = w/w_{sat} \tag{13}$$

The mean displacement $\overline{w}$ is normalised to the value at saturation w_{sat}, approximately 1mm. The constants C_1, C_2 of the numerator are found from the intersection of the asymptotes with the saturation displacement w_{sat}. The form of the denominator was chosen as a convenient means to model the rapid stiffness increase at saturation. Using the constants C_1, C_2, n_1=1, n_2=4, n_3=8 gives the dashed line labelled 'fit full profile', close to the indentation curve for the full profile.

5. STATIC PRESSURE v DISPLACEMENT

The pressure p_n for the envelope to reach displacement w_n is the sum of the pressure steps P_n, n=1…n. Each pressure step P_n is calculated from the mean of $K_{n\text{-}1}$ and K_n in Fig. 8, and the envelope step W_n, i.e.

$$p_n = \sum_{n=1}^{n} P_n,\ P_n = \frac{1}{2}\left(K_n + K_{n\text{-}1}\right)W_n \tag{14a,b}$$

The steps W_n, n=1 …n are taken from the reference envelope $\overline{w}_0$ at level n=0, when the pressure p_0=0. The step–wise integration was applied to the three strip profiles of Fig.6 with properties in Fg.7, yielding the three upper contact pressure against mean envelope displacement curves in Fig.9.

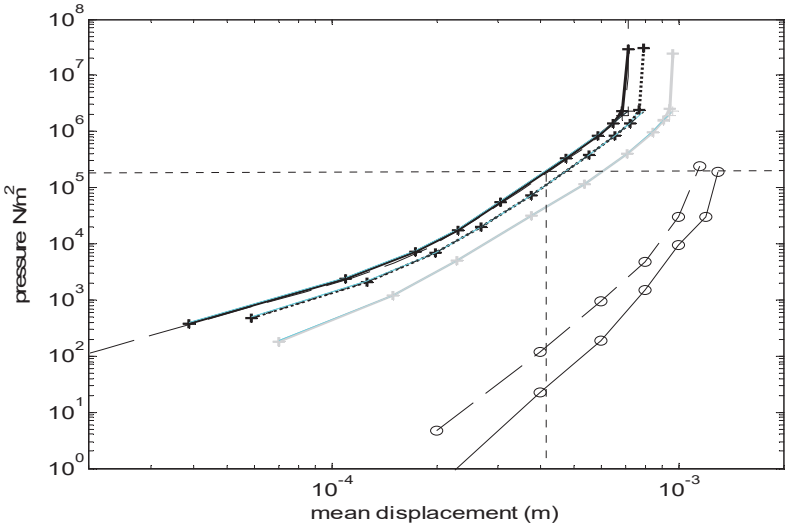

Figure 9- Contact pressure *v* displacement $\overline{w}_n$, ——— single profile, ... triple profile, ——— full profile, o---oconcrete surface (6), o—— o asphalt surface (6),– – – – fit to full profile

A typical operating pressure under a tyre p_{s0} was selected at $2\text{x}10^{-5}$N/m^2, indicated as the horizontal dotted line intersecting the three load curves between levels n=5 and n=6 at displacements of: 0.42mm, 0.49mm and 0.65mm for the 'full' profile, the 'triple' profile and 'single' profile respectively. As would be expected, increasing surface roughness increases displacement, for a given load.

From the assyptopic values of Fig.9 an empirical relationship for displacement in terms of pressure was obtained in terms of the normalised displacement $\overline{w}$ and normalised pressure $\overline{p}$, i.e.

$$\overline{w} = \left(1 + \frac{1}{\left(C_1\overline{p}^{4/7}\right)^n} + \frac{1}{\left(C_2\overline{p}^{1/4}\right)^n}\right)^{-1/n},\ \overline{w} = \frac{w}{w_{sat}},\ \overline{p} = \frac{p}{p_{sat}} \tag{15}$$

The saturation displacement and saturation pressure of the 'full'profile are respectively: w_{sat}=0.72mm, p_{sat}=2x10^{6}N/m^2. The function has three sections, an initial contact section of logarithmic slope 4/7, a main contact section of logarithmic slope ¼, and a displacement limit at w_{sat}. The constants C_1 and C_2 are found from the intersects of the two asymptotic curves with the saturation pressure. The integer n is only a device to control the rate of change in slope at the intersect between assyptopes, and was set at n=8 to for the fitted curve.

Also plotted in Fig.9 are some indentation measurements on concrete and asphalt surfaces (6), with peak height to the mean plane of 1.1mm and 1.4mm respectively, thus having about twice the roughness depth of the profiles used here. An exact correspondance was not expected because the measured surfaces were coarser and

less complex than those in the calculations. However at the operating pressure, the measured displacements are about twice the displacement of the calculated surface, as expected from a surface of about twice the depth, suggesting that the correct physical principles have been invoked in the calculations. It will be seen in the final section that the depth of contact at the operating pressure is the most important aspect of the contact.

6. ROLLING-TYRE FORCES

The complex problem, determination of rolling tyre contact force is approached by considering the road profile in two regions, as in Fig.1a and Fig.1b i.e. for wavelengths greater and less than twice the contact patch length respectively. The main simplifying assumption is the use of linear contact stiffness for the long wavelength model giving the tyre footprint pressure envelope that is then divided into point contacts by the short wavelength model.

6.1 Static pressure and displacement in the contact patch

To illustrate the method a simple rolling tyre model as in Fig.10 is used (7), consisting of a one-dimensional belt of unit width, and mass/m^2, M, subjected to a static tension /m, N, supported by a sidewall of linear stiffness/m^2, $K_w = 2K_{sw}/b$ the equivalent radial stiffness/area of the two sidewalls per belt width b.The vertical wheel load flattens the outer perimeter of the circular tyre by the static input displacement w_{s0}. The tyre is considered to be rolling to the left, causing the road profile w_r to pass through the static contact patch at speed c_r. The dynamic contact pressure $p(x,t)$ acts through the non-linear tread stiffness K_t stiffness/m^2 to give the tyre carcass displacement response w. Only tension and shear deformation is included but not bending, facilitating closed form algebraic solutions offering some physical understanding.

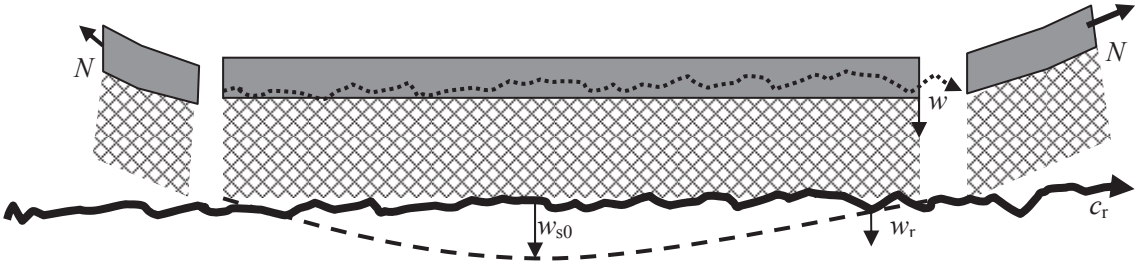

Figure.10- Section of a one-dimensional tyre in rolling contact with a road

The equation of motion for the displacement w is found from equilibrium of radial forces:

$$N\frac{\partial^2 w}{\partial x^2} - M\frac{\partial^2 w}{\partial t^2} - K_w w = p(x,t) \tag{16}$$

The pressure p applied to the belt via the tread, is in general a non-linear function in the relative displacement w_r-w, but if the tread stiffness K_t is assumed linear Eq.(16) becomes:

$$N\frac{\partial^2 w}{\partial x^2} - M\frac{\partial^2 w}{\partial t^2} - (K_t + K_w)w = -K_t w_r \tag{17}$$

The time variation is linked to the spatial variation by the vehicle speed c_r, i.e. $\partial t = \partial x / c_r$, which substituted into Eq.(17) yields: .

$$N\left(1 - \frac{c_r^2}{c^2}\right)\frac{\partial^2 w}{\partial x^2} - (K_w + K_t)w = -K_t w_{s0}, \quad c^2 = \frac{N}{M}, \quad K_t = \frac{K_{tr} + K_{s0}}{K_{tr}K_{s0}} \tag{18a,b,c}$$

The curvature term on the left has an elastic part described by the belt tension N in opposition to a dynamic part from the of the belt inertia M. Thus increasing speed effectively softens the tyre until c_r approaches the free belt wave speed c when the belt elasticity is entirely negated and a shock wave develops at the leading edge of the contact patch, leading to destruction of the tyre. Practical tyres are therefore built so that at normal driving speeds the elastic forces are always greater than the inertia forces. This implies that the belt inertia is not a dominant effect in contact force generation, and may thus be neglected.

The blocked pressure on the right of Eq.(18a) is the product of the input displacement w_{s0} and the linear stiffness K_t, defined in Eq.(18c) as the tread stiffness K_{tr} in series with the linear 'static contact stiffness' K_{s0} of 4.25x10^{8}N/m^2/m, found from Fig.9as as the pressure divided by the displacement at the operating load p_{s0} of

$2x10^5 N/m^2$. This definition of contact stiffness gives the true displacement at full load thus placing K_{s0} in correct overal relation to the other linear terms in Eq.(18a), leading to displacements and pressures of approximately the correct form.

The input w_{s0}, seen in Fig.10, is a segment of a circle of radius a, which for small displacements within the contact patch of length L_s, is approximately of the form i.e.

$$w_{s0} = a\left(1-\cos\left(2x/L_s\right)\right), \quad -L_s/2 \le x \le -L_s/2 \tag{18}$$

Solution of Eq.(18) yields the static displacements and pressure distribution $p_s(x)$, shown in Fig.11. The integral of the pressure over the contact patch (of length L_s=0.1m, and width b=0.14m), returns the vertical wheel load of about 2500N. The assumption of a linear static stiffness K_{s0}, will cause the initial displacement to rise too rapidly, before rising too slowly, as K_{s0} is about one quarter of the true, 'dynamic' stiffness K_{d0} at the operating load. However, the pressure distribution must always adjust so that the integral over the full contact length equals to the vertical wheel load, thus excessive errors in the total rise time,are not expected.

The static pressure $p_s(x)$ is substituted into the empirical non-linear load-displacement relationship of Eq.(15), yielding the displacement termed the'static envelope' $w_s(x)$ that appears almost as a box function. Division of the pressure distribution with the static envelope yields the distributed static stiffness $K_s(x)$:

$$K_s\left(x\right) = p_s\left(x\right)/w_s\left(x\right) \tag{19}$$

It is displayed in normalised form, as the grey line in Fig.11 along with the distributed 'dynamic stiffness' $K_d(x)$, found by substitution of the static envelope $w_s(x)$ into the empirical stiffness relationship, Eq.(13).

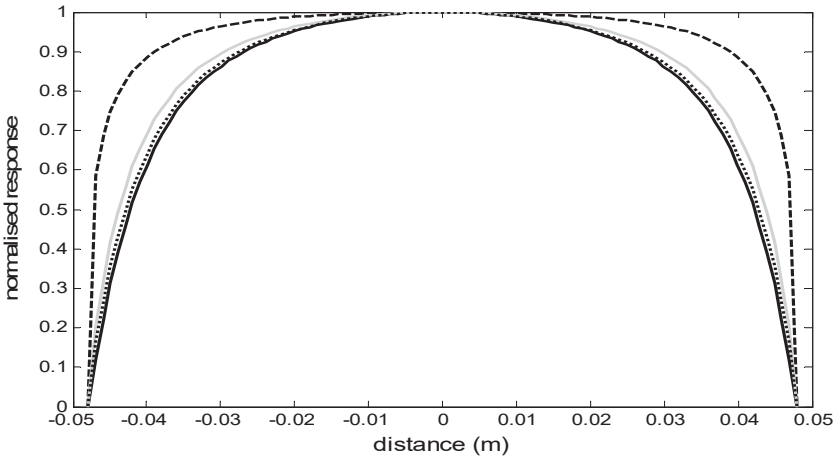

Figure 11- Pressure, stiffness and displacement of the tyre contact patch: _____ p_s static pressure normalised to p_{s0}= $1.8x10^5 N/m^2$, - - - - w_s.static envelope normalised to w_{s0} =0.415mm. ..... K_d dynamic stiffness normalised to K_{d0}=$1.5x10^9 N/m^2/m$, ——— K_s static stiffness, normalised to K_{s0}= $4.25x10^8 N/m^2/m$

The 'static envelope' corresponds to the mean penetration of the tyre tread into the road surface, and is used in the following sections to give the time varying contact forces, stiffness and displacement.

6.2 Long wavelength contact force and response

If it can be assumed that the surface is isotropic, it is possible to characterise the whole surface with just one strip profile, thus substantially reducing the surface data requirements. When a road is laid, there are long wavelength fluctuations in the direction of travel, modelled by the long wavelength profile w_L seen in Fig.12. Subsequent wear from traffic may cause fluctuations across the direction of travel, but these have greater wavelengths than twice the tyre width. Furthermore, across the road there is no rate of change from rolling in the direction of travel, and it is thus only necessary to assume that the road surface is isotropic over the range of the contact patch.

Long road wavelengths $\lambda > L_s$ are mainly responsible low frequency vibration and noise inside the vehicle, as the whole tyre contact patch is excited in phase as a single contact, efficiently transmitting vibration through the vehicle suspension. The long wavelength profile w_L includes all wavelengths greater than twice the contact length L_s, and it given as the envelope with a mean point spacing nearest to the contact length, (typically of 0.1m), corresponding (see Fig.7) to level n=1, i.e. envelope w_1. However the envelopes in this decomposition

are straight line segments between identified peaks, thus to avoid harmonics from the sudden change of slope, a cubic spline should be fitted between these points to give the smooth long wavelength profile w_L.

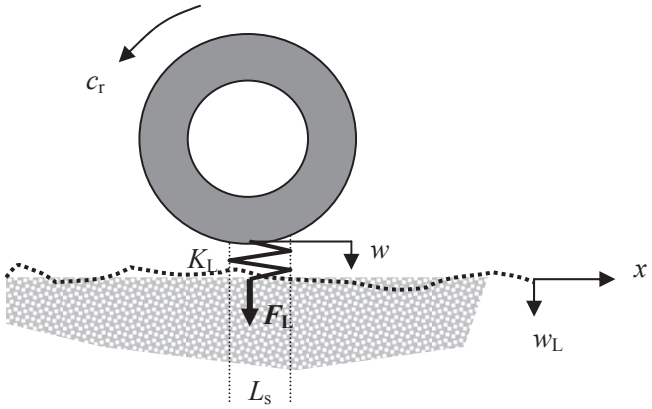

Figure 12- Long wavelength excitation of a rolling tyre

The long wavelength contact force and response w of a tyre of width b, to the long wavelength profile w_L, is calculated with reference to Fig.12. The contact force F_L acts equally on the tyre carcass of dynamic stiffness K_{tyre} and on the tread dynamic stiffness K_{d0} at the operating load, yielding the dynamic displacement w in terms of the profile w_L at position x and time t.i.e.

$$F_L = K_{tyre} w = K_L \left(w_L - w \right), \;\; K_L = bL_s K_{d0}, \; w = \frac{K_L w_L \left(x - c_r t \right)}{K_{tyre} + K_L} \tag{20a,b,c}$$

At these wavelengths, the contact patch stiffness tends to be greater than the tyre stiffness i.e. $K_L > K_{tyre}$ causing the tyre to follow the road profile, i.e. $w = w_L$ giving the contact force from Eq.(20a).

6.3 Short wavelength contact forces and responses

Sutraction of the long wavelength profile from the strip profile w_N leaves the short wavelengh profile w_{NL} describing only the roughness of stones in the contact patch i.e.

$$w_{NL} = w_N - w_L \tag{21}$$

Fig. 13 shows the static envelope, relative to the long wavelength envelope w_L, pushing a positive distance $w_s(x)$ into the the short wavelength profile w_{NL}. As the intersection of the mean envelope with the road profile was used to obtain the mean stiffness and mean contact pressures in Fig.(8,9), it is argued that the intersected area above the static envelope describes the contact forces from the individual peaks in the strip profile.

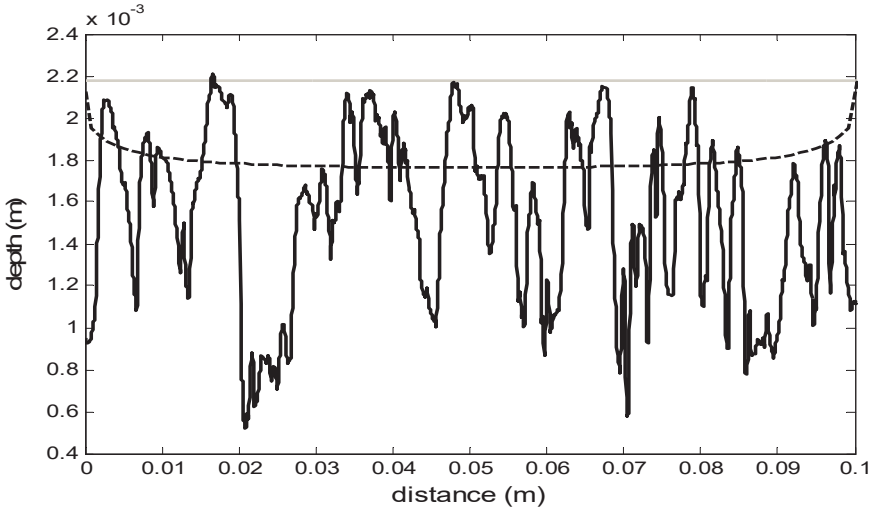

Figure 13- Displacement profiles in the contact patch: strip profile w_N Long wavelength envelope w_L, static envelope w_s

The profile w_{NL}, in distance x_r relative to the road, passes at speed c_r through the contact envelope, giving the penetration profile w_r:

$$\text{for } w_r \geq 0,\ w_r = w_{NL}\left(x_r - c_r t\right) + w_s\left(x\right);\ \ \text{if } w_r < 0, \text{ set } w_r = 0; \tag{22a,b}$$

When profile w_N is above the static envelope, there is contact as described by Eq.(22a), but if w_{NL} is below the static envelope, there is no contact, as in Eq.(22b), and the dashed line of the static envelope represents the free surface of the rubber. Thus the penetration into the surface roughness w_r, is the distance between profile w_{NL} and the dashed line of the static envelope w_s. For example, the first peak on the left has a penetration of about 0.2mm and a diameter of about 3mm. Outside of the contact patch i.e. $-L/2 > x > L/2$, the penetration w_r is zero, as there is no contact.

The intersection diameter of each peak with the static envelope yields the contact stiffness according to Eq.(1a), while the area above the static envelope yields the force at each point according to Eq.(1b). Thus Fig.13 provides the contact force, input displacement and stiffness on the tyre at one instant in time t. After a time Δt the profile w_{NL} moves to the right a distance $c_r \Delta t$, and the intersections with the the static envelope will change, the peaks on the left will intersect at a deeper levels giving a greater contact stiffness and force, while the peaks on the right will decrease in contact stiffness and force.

The contact forces and stiffnesses can be written in a suitable form to be included in a one-dimensional wave equation, i.e.

$$N\frac{\partial^2 w}{\partial x^2} - M\frac{\partial^2 w}{\partial t^2} = \frac{E^*}{\Delta}\left(w_r - w_r^0 w\right) \tag{23}$$

The tyre is normalised to unit width, so each term has units of pressure. The terms on the left, represent the dynamics of the free tyre, while the terms on the right are respectively the distributed contact pressures and stiffness, as a function of the penetration profile w_r and the strip width $\tilde{\Delta}$. For a single peak, the integral of w_r with respect to x gives the area under the peak, and hence the force from Eq.(1b). The second term on the right is the product of the contact stiffness and the tyre displacement w. The (contact stiffness)/(contact length) from Eq.(1a) is $2E^*a/(2a)$ i.e. E^*. Thus the device of w_r^0 gives unity over the length of each contact point, and zero out of contact, where w_r is zero. Although quite a compact equation, the moving contact stiffness in w_r, would only permit a solution in the time domain.

Usually only time averaged properties are required, giving some justification for using the average contact stiffness taken across the tyre width, that should remain in the region of the steady-state contact stiffness $K_d(x)$ of Fig.11. Eq.(23) then reduces to a linear wave equation, presented here in a two dimensional form for displacement $w(x,y,t)$, where y is in the cross-belt direction:

$$N_x\frac{\partial^2 w}{\partial x^2} + N_y\frac{\partial^2 w}{\partial y^2} - M\frac{\partial^2 w}{\partial t^2} + K_d\left(x\right)w = \frac{E^*}{\Delta}\sum_q w_{rq}\delta\left(y - q\Delta\right) \tag{24a}$$

On the left side, the elasticity of the global tyre is now represented by tensions N_x, N_y in the x and y directions. The dynamic contact stiffness K_d still has an awkward variation in x, but is independent of time. On the right side are the moving pressures. The belt across the contact patch is divided into strips of width Δ counted by integer q. The pressure from each strip is a delta function in the y direction. The pressure variation for each strip in the x direction in Eq.(24b), is almost the same as in Eq.(23) for the one dimensional case, except a shift term x_q is included, determining the start position on the profile w_{NL}, i.e.

$$\text{for } w_{rq} \geq 0,\ w_{rq} = w_{NL}\left(x_r + x_q - c_r t\right) + w_s\left(x\right);\ \ \text{if } w_{rq} < 0, \text{ set } w_{rn} = 0; \tag{24b}$$

As the statistical properties should be the same for any track in the direction of travel only one strip profile is enough to characterise the surface. If long enough it is therefore adequate to repeat the same sequence w_{NL} but randomly vary x_q, between tracks. When x_q is set at approximately $q\Delta$, the surface will be isotropic, i.e. have the same properties in the x and y directions. If this scheme was rigidly adhered to, the profiles would align on the 45^0 diagonal as they travelled through the contact patch. However since the contact forces are only controlled by the local elasticity, this should no influence at the contact line of the trailing and leading edges, where the main interaction occurs.

6. CONCLUSIONS

It was found that the indentation stiffness of particles with arbitrary shape could be estimated from the contact diameter, while contact forces are proportional to the vertical section area of the indented profile.

There is also deflection of the tyre belt between contact points due to bending and tension-shear, but for a typical tyre it appears that this is less than the indentation.

To obtain the mean properties of the measured road profile it was decomposed into a set of envelopes of decreasing search interval from the full record length to the data resolution level. The envelopes have two regimes separated by the particle level where the search interval corresponds to the particle spacing. For search lengths greater than particle spacing, the envelopes link the peaks at the chosen search interval, and so describe the relationship between the peaks. For search intervals shorted than the particle spacing, the envelopes work their way into the troughs between peaks, and so describe the particle shape.

A single measured road profile cuts the particles at arbitrary sections, and so often underestimates the peak heights. Thus a 'strip profile' was constructed to representing the true particle maxima within a strip with the width of the largest particle. Three profiles, within the strip width adequately represent the peaks for usual operating loads.

The mean properties of the strip profile were combined with the contact stiffness to give the stiffness-deflection relationship and pressure-displacement relationship for the surface. The predicted pressure-displacement curves showed similar trends to some measurements taken from the literature. However the measured surfaces were much coarser and so an exact comparison was not possible.

Rolling contact was analysed in two parts. The first part gave the steady-state pressure and envelope of the deflection in the tyre contact patch due the vertical wheel load. The second part found the time varying contact forces and contact stiffness from the intersection of the strip profile and the contact envelope. These terms were then configured in a rolling contact equation with a time and space varying stiffness. This was further reduced to a linear equation, although the contact stiffness still had a spatial variation.

ACKNOWLEDGEMENT

The author gratefully acknowledges the support for the ITARI project within the E.U. 6th Framework at the start of this study.

REFERENCES

1. Anderson PBU, Kropp W, Time domain contact model for tyre/road interaction including non-linear contact stiffness for small scale roughness, J. Sound Vib. 2008 (318) p.296-312
2. Pinnington RJ, Tyre-road contact using a particle-envelope surface model, J. Sound Vib. 2013, (332) p.7055-7075
3. Johnson KL, Contact Mechanics 1985, Cambridge University Press
4. Berry MV, Lewis ZV, On the Weierstrass-Mandlebrot fractal function, Proc. R.Soc, Lon. 1980 (A 370), p.459-484
5. Pinnington RJ, A wave model for a circular tyre (ii), sidewall and force transmission modelling. J. Sound Vib. 2006 (290) p.133-168
6. Lorenz B, Carbone G, Schulze C, Average separation between a rough surface and a rubber block, comparison between theories and experiments, 2009, Wear (268) p.984-990
7. Pinnington RJ. unpublished report